crystals

MDPI

Article

Microstructure, Hardness and EIS Evaluation of Ti-15Zr-5Nb Dental Alloy

Iosif Hulka [1,*], Julia C. Mirza-Rosca [2,3], Adriana Saceleanu [4] and Ion-Dragoș Uțu [5]

[1] Research Institute for Renewable Energy, Politehnica University Timişoara, G. Muzicescu 138, 300501 Timişoara, Romania
[2] Department of Mechanical Engineering, Las Palmas de Gran Canaria University, 35017 Tafira, Spain; julia.mirza@ulpgc.es
[3] Materials Engineering and Welding Department, Transilvania University of Brasov, 500036 Brasov, Romania
[4] Medicine Faculty, Lucian Blaga University of Sibiu, 550024 Sibiu, Romania; adriana.saceleanu@ulbsibiu.ro
[5] Department of Materials and Manufacturing Engineering, Faculty of Mechanical Engineering, Politehnica University Timișoara, Blvd. Mihai Viteazu, 300222 Timișoara, Romania; dragos.utu@upt.ro
* Correspondence: iosif.hulka@upt.ro

Abstract: Ti alloys have been widely used in biomedical applications due to their special properties. They have specific properties such as biocompatibility, biofunctionality and high corrosion resistance, which enable them to function inside the human body. Among them, Ti-6Al-4V is probably one of the most widely used alloys for implants. However, aluminum and vanadium ions have been reported to cause problems and adverse reactions in the human body over long periods. Thus, in the present study, Ti–15Zr–10Nb alloy synthesized by high vacuum melting was manufactured and characterized by different techniques. The phase composition was determined by XRD. This showed the presence of α and β phases in the alloy, consistent with the microstructural study. From a microstructural point of view, the alloy shows lamellar and acicular structures with α-grain boundaries. Vickers microhardness measurements showed an increased hardness compared to Ti-CP. Furthermore, the electrochemical behavior was evaluated using HCl as an electrolyte. The obtained results were compared to Ti-CP tested in the same electrochemical condition. The studies indicated that Ti-CP presents a nobler electrochemical behavior than Ti-15Zr-5Nb. Thus, despite the very good corrosion properties of Ti-15Zr-5Nb in a simulated oral environment and Ringer's solutions, the present study reveals that the Ti-15Zr-5Nb alloy has lower corrosion resistance in aggressive media when compared to Ti-CP.

Keywords: biomaterials; Ti–15Zr–10Nb; microstructure; hardness; EIS

Citation: Hulka, I.; Mirza-Rosca, J.C.; Saceleanu, A.; Uțu, I.-D. Microstructure, Hardness and EIS Evaluation of Ti-15Zr-5Nb Dental Alloy. *Crystals* **2024**, *14*, 602. https://doi.org/10.3390/cryst14070602

Academic Editor: Benilde F. O. Costa

Received: 5 June 2024
Revised: 26 June 2024
Accepted: 27 June 2024
Published: 29 June 2024

1. Introduction

In dentistry, the materials used in surgery are classified generally into dental implants, devices for maintaining the proper alignment of bone fragments that temporarily hold the load after a fracture of the mandible or maxilla, and devices for stabilizing bone fragments during orthognathic surgery [1]. Understanding the physical attributes of teeth and biological tissues is essential for the design of bio-functional metallic-based biomaterials as well as to understand their fundamental behavior [2]. Biomaterials must fulfill several requirements such as biocompatibility, osseointegration, low modulus of elasticity, corrosion resistance, fatigue strength and availability [3]. Because of these requirements, the use of metallic materials is quite limited to several groups which include stainless steel, commercially pure titanium (Ti-CP) and Ti-based alloys [4]. These include Ti alloys which exhibit the highest corrosion resistance, specific strength, and biocompatibility. In addition, Ti-based alloys are suitable alternatives to stainless steels and Co-Cr-based alloys used as implants because of lower elastic modulus which is crucial in inhibiting bone resorption and load transfer [5]. This group of alloys can be classified by the content of

the primary constitutional phase into: α, β and α + β alloys, with more subdivisions into near α and near β alloys [6]. Among them, the most used Ti-based alloy in the biomedical industry is the α + β type Ti–6Al–4V alloy. When Al and V are added to the composition the properties of the alloy are considerably improved compared to Ti-CP. However, there are still some issues with this alloy because it contains elements that are toxic for humans. Thus, V causes harmful tissue reactions and besides the reaction of V and Al ions within the human body might cause Parkinson's and Alzheimer's diseases [7]. In order to avoid this issue, Ti-Zr-Nb ternary alloys were studied as a biomaterial candidate for the manufacturing of implants. This alloy has the advantage of having a composition made entirely of non-toxic elements with excellent corrosion resistance. The most studied composition is Ti-13Nb-13Zr alloy which proved to have high corrosion resistance and to fulfill the requirement as biomaterial [8,9]. However, most ternary Ti-Nb-Zr alloys have some limitations. There have been attempts to overcome these problems by varying the percentage of constituents or by using different manufacturing methods to improve their properties [10]. Kęsik et al. showed that wollastonite promotes adhesion and proliferation of cells on the oxide layers formed on the Ti–13Nb–13Zr alloy surface improved by using a plasma electrolytic oxidation process [11]. Kumar et al. increased the corrosion resistance through grain refinement at the surface of Ti-13Nb-13Zr alloy by using ultrasonic shot peening [12]. Different manufacturing methods were used to prepare Ti-13Nb-13Zr alloys with improved properties. Selective laser melting [13], filtered arc deposition [14], laser-based Powder Bed Fusion [15], mechanical alloying and spark plasma sintering [16], and high vacuum consume electric arc melting followed by heat treatment [17] are the main methods used by researcher to manufacture Ti-13Nb-13Zr. To further improve the alloy's properties, Moreno et al. manufactured Ti-15Zr-5Nb alloy by slightly increasing the Zr content and lowering the amount of Nb obtaining an alloy with an elastic modulus of about 83 GPa [18]. It was found that the new alloy revealed a nobler behavior than Ti-CP and Ti-6Al-4V in simulated body fluid and artificial saliva, overall satisfying the most important requirements of an implant material [19]. In addition to body fluids, sometimes the implant comes into contact with beverages as well which has a negative impact on the material. Nowadays, carbonated drinks containing acids such as phosphoric acid are consumed in quite high amounts, especially, by the younger generation leading to tooth demineralization [20]. Furthermore, Sankar et al. reported that there is a significant surface change in dental materials when exposed for longer periods of time to low pH drinks such as cola and orange juice due to the presence of phosphoric and citric acid, respectively [21].

Several articles can be found dealing with the mechanical properties and corrosion behavior of Ti-15Zr-5Nb in ringer solution without the material being tested in other environments. Since this particular alloy presents enhanced mechanical properties combined with enhanced corrosion resistance in simulated body fluids it is of interest to further study its electrochemical behavior in different electrolytes.

Therefore, the aim of our work is to conduct a comprehensive study of the mechanical properties and to study the corrosion behavior of the Ti-Zr-Nb alloy in an aggressive acidic media such as HCl electrolyte through electrochemical techniques. Thus, Ti-15Zr-5Nb alloy was obtained in an as-cast state by double vacuum melting in a cold crucible.

X-ray diffraction (XRD) was employed to perform phase analysis. The microstructure was evaluated by means of optical (OM) and scanning electron microscopy (SEM) techniques combined with energy-dispersive X-ray analysis (EDX). The mechanical properties in terms of hardness were evaluated as well. The novelty of the work is to further investigate the corrosion behavior of Ti-Zr-Nb alloy in an aggressive acidic media such as HCl by means of electrochemical techniques such as Cyclic Voltammetry (CV) and Electrochemical Impedance Spectroscopy (EIS). The obtained results were compared to Ti-CP tested in the same conditions. We considered that this might be of interest to researchers in the field of materials science, dentistry, and electrochemistry since the influence of HCl on the corrosion resistance of Ti-15Zr-5Nb alloy has not reported so far according to our knowledge.

2. Materials and Methods

2.1. Ti-15Zr-5Nb Alloy Preparation

The alloy investigated in the present study was prepared in an as-cast state by using a double vacuum electronic flow melting oven (Emo 80, ZIROM S.A. Giurgiu, Romania) from Ti, Zr and Nb powders. From the obtained ingot, cylindrical samples were cut to prepare them for microstructural characterization, hardness measurements, and electrochemical measurements. In order to prepare the samples for metallography and hardness measurements, the procedure consisted of hot mounting in carbon-based resin, grinding the samples up to 2400 grit SiC paper, followed by polishing with alpha alumina of 0.1 µm until a mirror-like surface was obtained.

2.2. Characterization

The samples were ultrasonically cleaned using deionized water and etched in Kroll's reagent for 15 s of immersion time. A metallographic microscope (Olympus PME 3-ADL, Olympus, Tokyo, Japan) was employed for optical metallographic observations. To investigate the microstructure of the alloy a scanning electron microscope (FE-SEM Zeiss Sigma 300 VP, Carl Zeiss, Jena, Germany) coupled with an energy-dispersive X-ray spectrometer (EDS) was used. The SEM micrographs were acquired in high-vacuum mode, at a cathode voltage of 15 kV at a working distance of about 10 mm. A backscattered electron detector (BSD) was used to reveal the different phases within the sample by using Z contrast. EDS was performed for chemical characterization by positioning the sample at an eucentric height.

The constituent phase of the Ti-15Zr-5Nb alloy was identified by XRD on an Empyrean diffractometer (Malvern–Panalytical Empyrean, Almelo, The Netherlands) using Cu Kα radiation. The measurements were performed at room temperature at a 2θ angle in the range of 30–80° using a power of 40 kV and 30 mA.

The microhardness measurements were performed using a Buehler Micromet VD 5124 (Buehler, Lake Bluff, IL, USA) hardness tester with a Vickers indenter. A total of 10 indents were taken using a load of 200 gf with a 15 s holding time.

For electrochemical measurements, the samples were cut and embedded in carbon-based resin to protect the edges during grinding and polishing. Afterward, a copper wire was attached to the sample as presented in Figure 1 to assure electrical contact between the working electrode and the potentiostat during the electrochemical measurements.

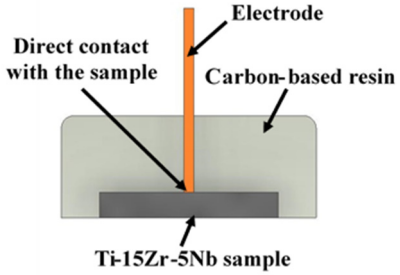

Figure 1. Schematic representation of the Ti-15Zr-5Nb sample mounted in resin for corrosion tests.

The electrochemical behavior of Ti-15Zr-5Nb and Ti-CP was investigated using CV and EIS using a Biologic SP-150 potentiostat (BioLogic Science Instruments, Seyssinet-Pariset, France). The electrochemical experiments were conducted at a temperature of around 22 °C, by using a standard electrochemical glass cell containing 350 mL of HCl solution with a pH of 2.5. Even though the normal acidity of the oral cavity is higher, a low pH was chosen for the study because it is of interest to analyze the behavior of the alloy in extremely severe conditions. Moreover, most carbonated drinks have this pH. The fresh drinks are taken between 5 and 8 °C and the temperature of the oral cavity decreases, remaining for a certain time at much lower values than the normal body temperature. The working electrode's potential was determined relative to a saturated calomel electrode (SCE) immersed in

potassium chloride (KCl) solution. Platinum gauze served as the counter electrode. Before testing, each electrode was maintained at −1.5V for 15 min to reduce any oxides developed on the surface of tested samples. The CV was assessed at a potential in the range of −1.5V to 2.5V vs SCE with a potential step rate of 10, 50, 100 and 200 mV/s. The recorded EIS data were fitted with an equivalent circuit by using the Lavenberg–Marquardt methods and ZView 2 software (Scribner Associates, Inc., Southern Pines, NC, USA).

3. Results and Discussions

3.1. Microstructure

Figure 2 presents the XRD pattern of the investigated alloy. The structure of the alloy consists of two main crystalline phases as follows: the α phase with a hexagonal closed pack structure and the β phase with a body-centered cubic structure.

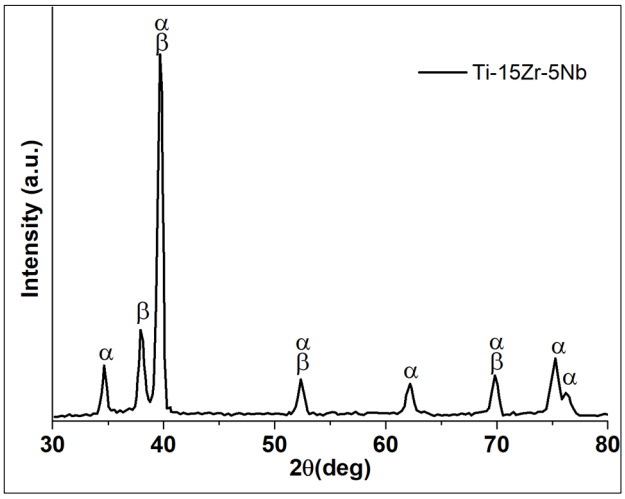

Figure 2. XRD diffraction pattern for the Ti-15Zr-5Nb alloy.

The microstructure of the investigated alloy after metallographic preparation is presented in Figure 3. The material consists of α and β phases which is in agreement with the XRD analysis. The etchant colors the β phase dark brown while the α phase resembles a shade of light gray. Since there is a potential difference between the phases, the differences alter the rate of attack and reveal the microstructure when chemical etchants are used. In a two-phase alloy, the potential of one phase is greater than that of the other. During etching, the more electropositive (anodic) phase is attacked (the β phase), while the more electronegative (cathodic) phase is not significantly attacked (the α phase) [22]. The α phase presents two types of morphologies as presented in Figure 3b. Thus, the identified α phases within the microstructure are namely: lamellar α phase (α) which predominates the microstructure, and a secondary acicular phase (α_a). In addition, the α phase nucleates during cooling and is encountered at grain boundaries. Generally, the β phase presents a lamellar microstructure in which the α is embedded. The lamellar microstructure is attributed to the solidification process which is responsible for the shape and size of the lamellas as well as for the formation of α grain boundaries. The parallel α lamellas within a colony indicate a deformation in a similar way formed from the same β parent grain. In addition, the α and β phases no other phases nor precipitates were identified by using metallographic characterization. In comparison with the findings reported by Moreno et al. when studying the microstructure and electrochemical behavior of Ti-15Zr-5Nb alloy obtained by vacuum melting [10], besides the lamellar microstructure in our study acicular α was identified as well at some grains next to the grain boundaries. The acicular morphology is attributed to the martensitic transformation which depends only on the cooling rate [23].

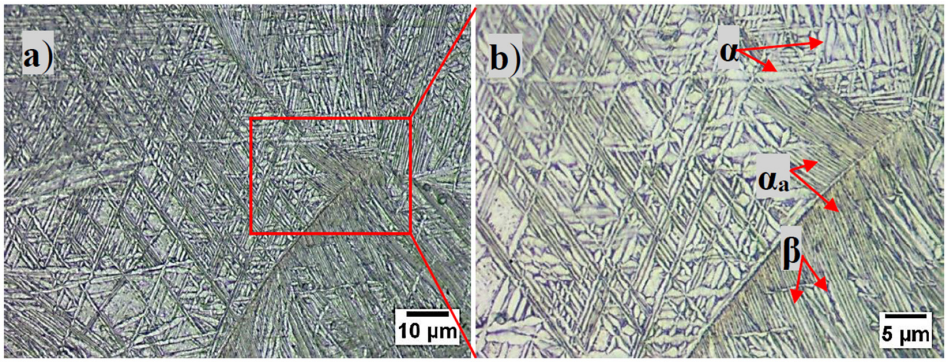

Figure 3. Optical micrographs of Ti-15Zr-5Nb alloy at lower magnification revealing general microstructure (**a**) and at higher magnification revealing fine acicular microstructure and α rich grain boundaries (**b**).

The lamellar microstructure and grain boundary were revealed in Figure 4a by the SEM micrographs. The microstructure of the material consisted of lamellar α in a transformed β matrix. In addition, a continuous grain boundary rich in α phase was noticed accompanied from place to place by the β phase next to it. EDS point analysis was used to investigate the chemical composition of the sample as shown by the representative elemental spectra and quantification presented in Figure 4b,c. The results reveal the present of constituent elements such as Ti, Zr, Nb and O. The presence of oxygen is attributed to the formation of a spontaneous oxide film which develops on Ti alloys when exposed to the environment. One can notice that Area 1, associated with the α phase, is richer in Ti while Area 2, associated with the β phase, has a lower amount of Ti and is enriched in alloying elements. This is attributed to the fact that Nb and Zr are β-stabilizers, which aim to stabilize the β-structure by lowering the transition temperature in Ti alloys [24]. Following the rule of stability, β-stabilizers have an affinity to the β phase and similar observations were reported by Yu et al. when investigating the corrosion behavior of Ti6Al4V in HCl solution [25] and by Avad et al. when studying the microstructure of heat-treated Ti6Al7Nb alloys [26].

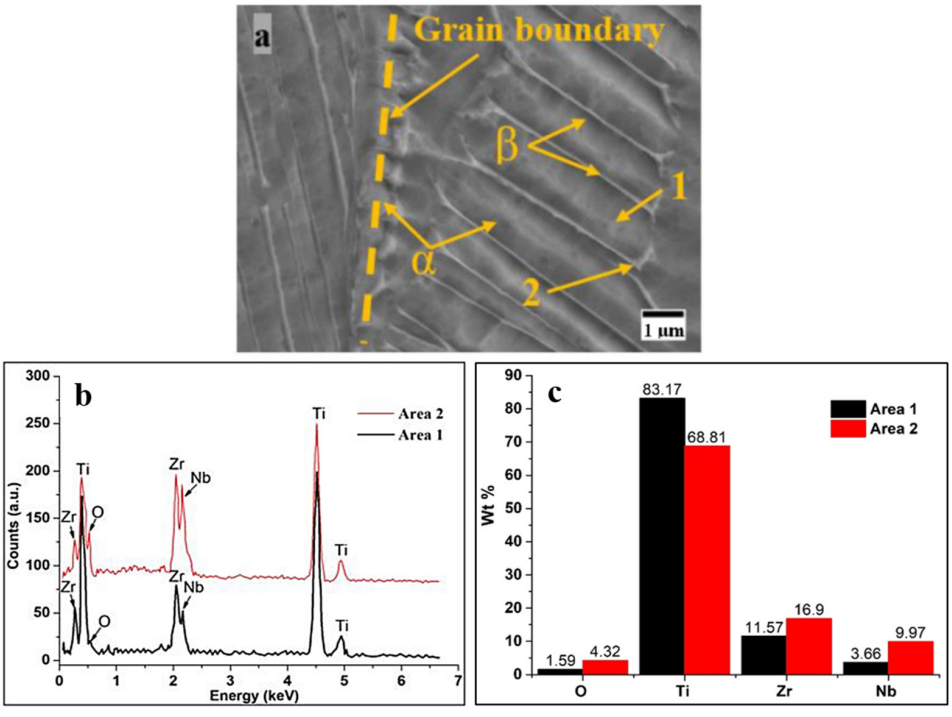

Figure 4. SEM—high magnification of acicular structure (**a**), EDS spectra (**b**), and associated quantification (**c**).

3.2. Microhardness

The microhardness test was carried out using a load of 200 gf and the results are summarized under graph form in Figure 5. It can be seen that the average HV value was 231.9 ± 6.28 which is bigger than the microhardness of Ti-CP which is 210 HV tested under the same conditions [27]. The fluctuations in the measurements are caused do the differences of hard and soft regions ascribed to the α and β phases identified within the microstructure [28].

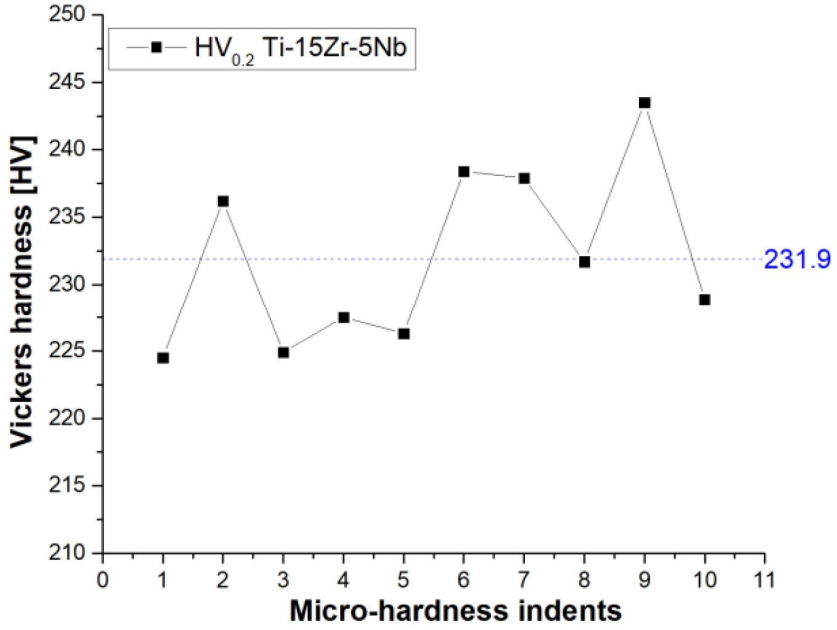

Figure 5. Hardness measurements of Ti-15Zr-5Nb alloy under 200 gf load.

3.3. Electrochemical Behavior

CVs were performed on Ti-15Zr-5nb and Ti-CP at different potential sweep rates in the range of 50 mV/s up to 500 mV/s between −1.5 V and 2.5 V vs SCE to determine the potential ranges of different electrochemical reactions of the samples in HCl electrolyte and the results are presented in Figure 6. Moreover, their kinetic features were assessed to determine the most appropriate conditions for the potentiostatic study of corrosion reactions. Figure 6 presents the CVs of Ti-15Zr-5Nb and it can be observed that the potential rises above 2.2 V vs. SCE at a sweep rate of 50 mV/s, the current increases abruptly to an elevated value indicating the deterioration of the passive film and the initiation of pitting corrosion of the samples. Thus, this potential is equivalent to the transpassivation potential threshold. The anodic current increased steadily as the potential sweep rates increased, making the passive film stronger against damage due to the increase in film thickness while no film breakdown was noticed. Similar circumstances were observed for the Ti-CP sample at all potential sweep rates, with a current plateau extended to the end of the potential values. As the potential ascends from −1.5 V vs. SCE, the anodic current increases for both samples, with anodic peaks that eventually merge into one, a higher and larger peak as the potential sweep rate increases. These anodic peaks are related to the following Ti oxidation reaction as presented by Pourbaix [29]:

$$Ti \rightarrow Ti^{2+} \rightarrow Ti^{3+} \rightarrow Ti^{4+} \quad (1)$$

In a strong acid environment, the anodic reaction of Zn is very easy to occur leading to a reduced corrosion resistance of Zr [30].

$$Zr\ (m) \rightarrow Zr^{4^*}(a{\cdot}q) + 4^{e-} \quad (2)$$

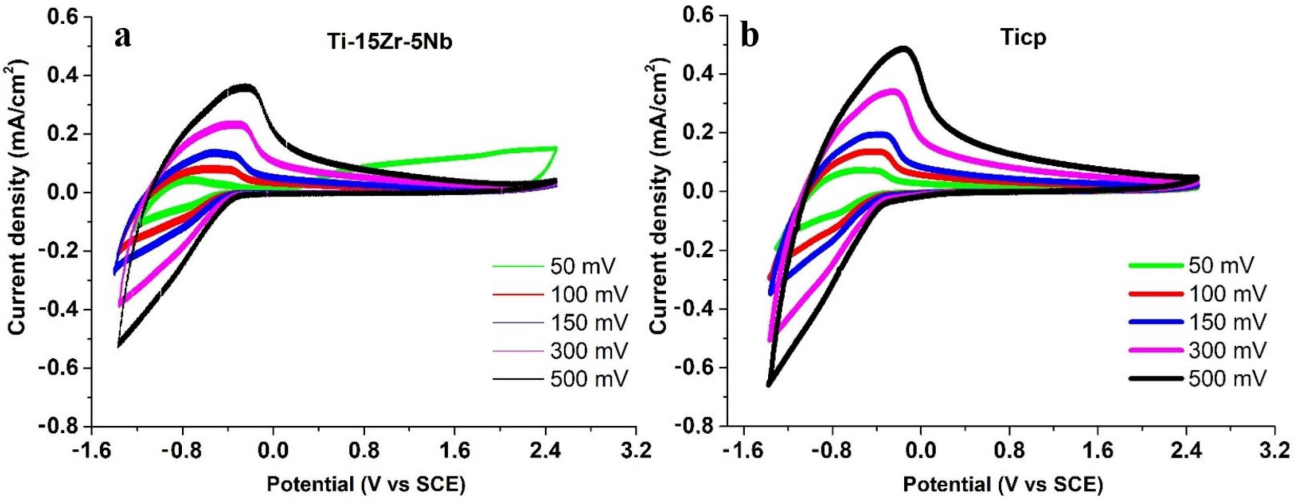

Figure 6. Cyclic voltammetry of Ti-15Zr-5Nb alloy (**a**) vs. Ti-CP (**b**) in HCl.

Even Nb_2O_5 is a known lubricant and ductile oxide which can significantly increase the corrosion resistance [31] of the alloy in the present case, due to a lower concentration, it does not influence the corrosion behavior of the alloy.

EIS is a strong analytical technique used to investigate the electrochemical behavior that takes place at the interface of a material immersed in an electrolyte. The technique is used in corrosion analysis to understand the behavior of metals and alloys as they deteriorate due to the electrochemical process. The Nyquist plots presented in Figure 7 present impedance data in the context plane which provide significant insights into the electrochemical behavior of surface-electrolyte system. The diameter of the semi-circle presents the system's charge transfer resistance (Rct). Moreover, because of the formation of a protective film on the surface of the sample, a large diameter suggests that it has greater transfer resistance. The center of the semi-circle is frequently near to the real axis indicating that the solution resistance (Rs) is minimal.

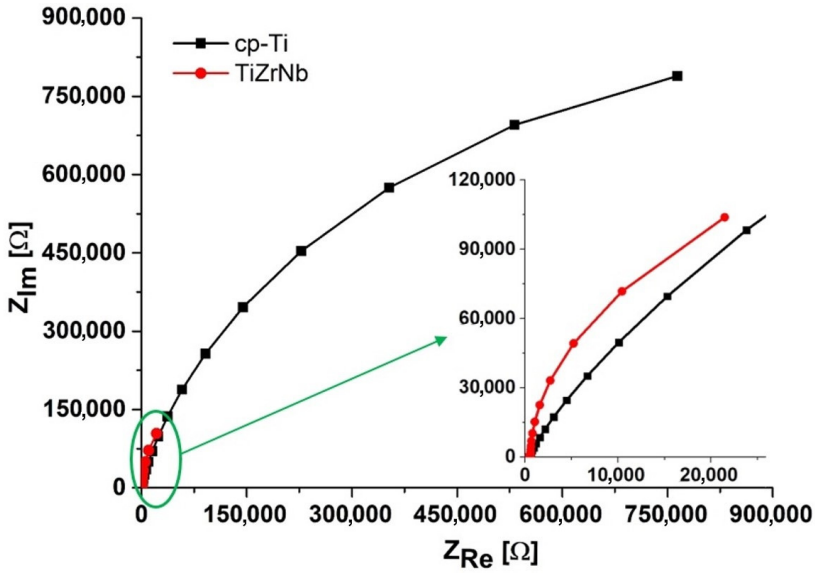

Figure 7. Nyquist diagrams of Ti-CP and Ti-15Zr-5Nb tested in HCl.

At the corrosion potential of the Bode-Phase diagram, the typical behavior of the initial nucleation of passive film on the metal's surface can be observed in Figure 8. The developed film on the sample's surface has a capacitive response as shown by a phase

angle close to 90 degrees across a wide frequency range. This phenomenon is tied to an increase in capacity which is linked to an increase in effective surface area.

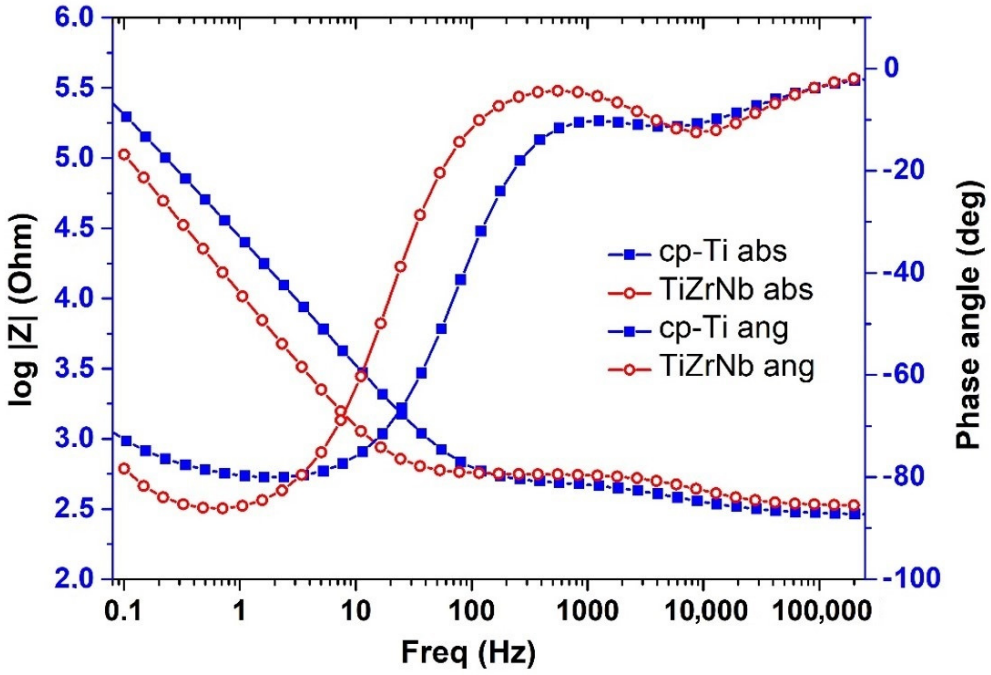

Figure 8. Bode diagrams of Ti-CP and Ti-15Zr-5Nb tested in HCl.

After analyzing the profiles of the impedance spectra, the experimental data were translated to an analogous electrical model. An analogous circuit is a collection of passive components (resistance, inductors, capacitances and other types of distributed impedances) that demonstrate corrosion-like behavior in the frequency range under consideration. The constant phase element (CPE) introduced by Boukamp [32] leads to better results. Thus, it is an adjustable element in electrical equivalent circuits that can detect a broad spectrum of electrochemical behavior in impedance spectroscopy, particularly those including non-ideal capacitive, inductive, and resistive characteristics. Its value labeled "n" allows for continuous phase angle adjustment leading to a more accurate illustration of complex electrochemical systems. The response of the real system is closer to the ideal one because the value of "n" is close to the unit and the surface is more uniform. As a result, for n = 0, the CPE element is a simple resistance, and for n = 1, it is a capacitor with capacitance Y^0. In the present work, the circuit presented in Figure 9 was used with the following elements to fit the EIS experimental data:

- Solution resistance (Rs)—caused by the electrolyte through which the current flows;
- CPEp—corresponds to the external passive film;
- Rp—resistance attributed to the external film;
- CPEc—corresponds a compact inner passive film;
- Rc—represents the alloy's polarization resistance.

From the fitted results presented in Table 1, it can be observed that the resistance against the aggressive HCl environment, Ti-15Zr-5nb alloy is a few times less compared to the Ti-CP.

Table 1. Electrochemical parameters of equivalent circuit.

Sample	R_s [$\Omega \cdot cm^2$]	Y_o [$\Omega^{-1} \cdot cm^{-2} \cdot s^{-n}$]	n	R_p [$\Omega \cdot cm^2$]	Y_o [$\Omega^{-1} \cdot cm^{-2} \cdot s^{-n}$]	n	R_c [$\Omega \cdot cm^2$]	χ^2
Ti-CP	285.4	2.98×10^{-6}	0.72	246.9	4.31×10^{-6}	0.97	2.21×10^{6}	2.5×10^{-3}
Ti-15Zr-5Nb	334.1	3.42×10^{-7}	0.88	232.1	1.43×10^{-5}	1	5.48×10^{5}	3.2×10^{-2}

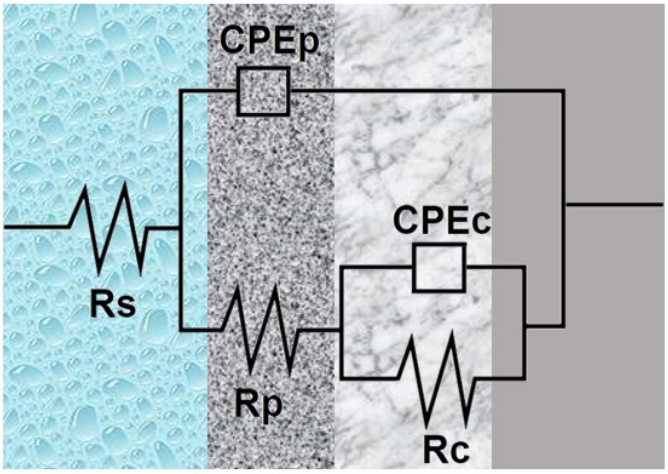

Figure 9. Electrical circuit used for data fitting.

4. Conclusions

In the present study, the microstructure, phases and the influence of the applied load on the microhardness of Ti-15Zr-5Nb dental alloy were investigated. In addition, the corrosion resistance in HCl electrolyte was evaluated by means of electrochemical techniques and the obtained results were compared to Ti-CP tested in the same conditions. The experimental results lead to the following conclusions:

- The structural analysis combined with the microscopic observations indicated that Ti-15Zr-5Nb is a biphasic alloy with the α phase having a hexagonal closed-package structure and the β phase having a body-centered cubic structure with lamellar and acicular structures and α grain boundaries. The microstructure is attributed to the solidification process which is responsible for the shape and size of the lamellas as well as for the formation of α rich grain boundaries.
- The β is enriched in alloying elements such as Nb and Zr which are β phase stabilizing elements.
- The hardness measurements revealed an increased hardness compared to Ti-CP with fluctuations caused due to the differences of hard and soft regions ascribed to the α and β phases identified within the microstructure.
- Despite the very good corrosion properties of Ti-15Zr-5Nb in simulated body fluids, compared to Ti-CP reported by other authors, the present study reveals that the Ti-15Zr-5Nb alloy has lower corrosion resistance in a strong acid environment compared to Ti-CP.
- From the results of the fitting, it was observed that the resistance against corrosion of the Ti-15Zr-5Nb in an aggressive environment such as HCl was a few times less compared with that of Ti-CP.

Author Contributions: Conceptualization, I.H. and J.C.M.-R.; methodology, I.H.; software, I.-D.U.; validation, A.S. and J.C.M.-R.; formal analysis, I.-D.U.; investigation, I.H. and I.-D.U.; resources, A.S.; data curation, writing—original draft preparation, I.H.; writing—review and editing, I.-D.U. and J.C.M.-R.; visualization, A.S.; supervision, A.S. All authors have read and agreed to the published version of the manuscript.

Funding: This research received no external funding.

Data Availability Statement: The original contributions presented in the study are included in the article, further inquiries can be directed to the corresponding author.

Conflicts of Interest: The authors declare no conflict of interest.

References

1. John, K.R.S. Mechanical biocompatibility of dental materials. In *Biocompatibility of Dental Biomaterials*; Elsevier: Amsterdam, The Netherlands, 2017; pp. 9–21. [CrossRef]
2. Niinomi, M. Mechanical biocompatibilities of titanium alloys for biomedical applications. *J. Mech. Behav. Biomed. Mater.* **2008**, *1*, 30–42. [CrossRef]
3. Eliaz, N. Corrosion of metallic biomaterials: A review. *Materials* **2019**, *12*, 407. [CrossRef] [PubMed]
4. Warlimont, H. Titanium and Titanium Alloys. In *Handbook of Materials Data*; Springer: Cham, Switzerland, 2018; pp. 199–210. [CrossRef]
5. Niinomi, M.; Nakai, M.; Hieda, J. Development of new metallic alloys for biomedical applications. *Acta Biomater.* **2012**, *8*, 3888–3903. [CrossRef]
6. Agrawal, C.M.; Ong, J.L.; Appleford, M.R.; Mani, G. *Introduction to Biomaterials*; Cambridge University Press: Cambridge, UK, 2013. [CrossRef]
7. Khadija, G.; Saleem, A.; Akhtar, Z.; Naqvi, Z.; Gull, M.; Masood, M.; Mukhtar, S.; Batool, M.; Saleem, N.; Rasheed, T.; et al. Short term exposure to titanium, aluminum and vanadium (Ti 6Al 4V) alloy powder drastically affects behavior and antioxidant metabolites in vital organs of male albino mice. *Toxicol. Reports* **2018**, *5*, 765–770. [CrossRef]
8. Niemeyer, T.C.; Grandini, C.R.; Pinto, L.M.C.; Angelo, A.C.D.; Schneider, S.G. Corrosion behavior of Ti-13Nb-13Zr alloy used as a biomaterial. *J. Alloys Compd.* **2009**, *476*, 172–175. [CrossRef]
9. Cvijović-Alagić, I.; Cvijović, Z.; Mitrović, S.; Panić, V.; Rakin, M. Wear and corrosion behaviour of Ti-13Nb-13Zr and Ti-6Al-4V alloys in simulated physiological solution. *Corros. Sci.* **2011**, *53*, 796–808. [CrossRef]
10. Moreno, J.C.; Vasilescu, E.; Drob, P.; Osiceanu, P.; Vasilescu, C.; Drob, S.; Popa, M. Surface and electrochemical characterization of a new ternary titanium based alloy behaviour in electrolytes of varying pH. *Corros. Sci.* **2013**, *77*, 52–63. [CrossRef]
11. Kazek-Kesik, A.; Krok-Borkowicz, M.; Jakóbik-Kolon, A.; Pamuła, E.; Simka, W. Biofunctionalization of Ti-13Nb-13Zr alloy surface by plasma electrolytic oxidation. Part II. *Surf. Coatings Technol.* **2015**, *276*, 23–30. [CrossRef]
12. Kumar, P.; Mahobia, G.S.; Mandal, S.; Singh, V.; Chattopadhyay, K. Enhanced corrosion resistance of the surface modified Ti-13Nb-13Zr alloy by ultrasonic shot peening. *Corros. Sci.* **2021**, *189*, 109597. [CrossRef]
13. Zhou, L.; Yuan, T.; Li, R.; Tang, J.; Wang, G.; Guo, K.; Yuan, J. Densification, microstructure evolution and fatigue behavior of Ti-13Nb-13Zr alloy processed by selective laser melting. *Powder Technol.* **2019**, *342*, 11–23. [CrossRef]
14. Li, J.; Zhang, Y.; Zhao, Y. Mechanical properties of TiN ceramic coating on a heat treated Ti-13Zr-13Nb alloy. *J. Alloys Compd.* **2017**, *724*, 34–44. [CrossRef]
15. Hoppe, V.; Pawlak, A.; Szymczyk-Ziółkowska, P.; Jaśkiewicz, T.; Rusińska, M.; Dybała, B. Investigation of Ti-13Nb-13Zr alloy powder properties and development of the L-PBF process. *Mater. Des.* **2022**, *217*, 110546. [CrossRef]
16. Kong, Q.; Lai, X.; An, X.; Feng, W.; Lu, C.; Wu, J.; Wu, C.; Wu, L.; Wang, Q. Characterization and corrosion behaviour of Ti-13Nb-13Zr alloy prepared by mechanical alloying and spark plasma sintering. *Mater. Today Commun.* **2020**, *23*, 101130. [CrossRef]
17. Shi, A.; Cai, D.; Hu, J.; Zhao, X.; Qin, G.; Han, Y.; Zhang, E. Development of a low elastic modulus and antibacterial Ti-13Nb-13Zr-5Cu titanium alloy by microstructure controlling. *Mater. Sci. Eng. C* **2021**, *126*, 112116. [CrossRef] [PubMed]
18. Moreno, J.M.C.; Vasilescu, C.; Drob, S.I.; Neacsu, E.I.; Popa, M. Evaluation of the microstructural, mechanical and anti-corrosive properties of a new ternary Ti–15Zr–5Nb alloy in simulated oral environment. *Mater. Corros.* **2014**, *65*, 703–714. [CrossRef]
19. Moreno, J.M.C.; Vasilescu, C.; Drob, S.I.; Popa, M.; Drob, P.; Vasilescu, E. Electrodeposition, characterization, and corrosion stability of nanostructured anodic oxides on new Ti-15Zr-5Nb alloy surface. *J. Nanomater.* **2013**, *2013*. [CrossRef]
20. Liu, M.; Li, J.; Li, D.; Zheng, L. The passive properties of TA10 in Coca-Cola containing oral environment. *Anti-Corrosion Methods Mater.* **2021**, *68*, 9–16. [CrossRef]
21. Sankar, A.; Kumar, M.; Kumar, K.; Pranitha, K.; Kishore, K.; Rajavardhan, K. Erosive potential of cola and orange fruit juice on tooth colored restorative materials. *Ann. Med. Health Sci. Res.* **2014**, *4*, 208. [CrossRef] [PubMed]
22. Radzikowska, J.; Stachailczyk, J. Application of Color Metallographic Techniques to Study the Microstructure of Titanium Alloys. *Sci. Technol.* **1999**, *6*, 13–19.
23. Gheorghe, D.; Pop, D.; Ciocoiu, R.; Trante, O.; Milea, C.; Mohan, A.; Benea, H.; Saceleanu, V. Microstructure development in titanium and its alloys used for medical applications. *UPB Sci. Bull. Ser. B Chem. Mater. Sci.* **2019**, *81*, 244–258.
24. Pesode, P.; Barve, S. A review—Metastable β titanium alloy for biomedical applications. *J. Eng. Appl. Sci.* **2023**, *70*, 25. [CrossRef]
25. Yu, F.; Addison, O.; Davenport, A. Temperature-Dependence Corrosion Behavior of Ti6Al4V in the Presence of HCl. *Front. Mater.* **2022**, *9*, 880702. [CrossRef]
26. Awad, A.H.; El-Hadad, S.; Ahmed, M.; Elshaer, R.N. Effects of Multistage Aging Treatment on the Microstructure and Mechanical Properties of α + β-Type Ti-6Al-7Nb Alloy. *J. Mater. Eng. Perform.* **2023**, *32*, 11367–11380. [CrossRef]
27. Kahraman, N.; Gülenç, B.; Findik, F. Joining of titanium/stainless steel by explosive welding and effect on interface. *J. Mater. Process. Technol.* **2005**, *169*, 127–133. [CrossRef]
28. Hulka, I.; Uțu, I.-D.; Brito-Garcia, S.; Verdu-Vazquez, A.; Mirza-Rosca, J.C. Electrochemical Study and Mechanical Properties of Ti-Zr Alloy for Biomedical Applications. *Crystals* **2024**, *14*, 493. [CrossRef]
29. Pourbaix, M. *Atlas of Electrochemical Equilibria in Aqueous Solutions*, 2nd ed.; National Association of Corrosion: Houston, TX, USA, 1974.

30. Peng, D.; Bai, X.; Pan, F.; Sun, H.; Chen, B. Influence of titanium ions implantation on corrosion behavior of zirconium in 1 M H_2SO_4. *Appl. Surf. Sci.* **2006**, *252*, 2196–2203. [CrossRef]
31. Pauline, S.A.; Rajendran, N. Corrosion behaviour and biocompatibility of nanoporous niobium incorporated titanium oxide coating for orthopaedic applications. *Ceram. Int.* **2017**, *43*, 1731–1739. [CrossRef]
32. Boukamp, B.A. A Nonlinear Least Squares Fit procedure for analysis of immittance data of electrochemical systems. *Solid State Ionics* **1986**, *20*, 31–44. [CrossRef]